COMPOSITE MATERIALS FATIGUE ISSUES IN WIND TURBINE BLADE CONSTRUCTION

John F. Mandell, Daniel D. Samborsky, and Pancasatya Agastra
Department of Chemical and Biological Engineering, Montana State University,
Bozeman, MT 59717

ABSTRACT

This paper provides an overview of the results of recent studies of composite laminates of interest for wind turbine blade construction. In addition to the primary requirements of stiffness, strength, and ease of processing, wind blade materials must withstand severe fatigue loading under service environments. The large material volumes and cost constraints also lead to unusually thick plies and fabrics, as well as thick adhesive bonds, which, combined with relatively brittle, low cost resins, can exacerbate delamination related structural integrity issues found in most composites structures. Important differences in performance are shown for the major fiber and resin types of relevance to blades. Details of fabric construction, fiber content and ply drop and geometry can produce major differences in performance, particularly under fatigue loading. Materials and conditions are identified where particularly low strain damage failure can occur at high cycles.

KEY WORDS: Fatigue, Wind Turbine Blade Technology, Glass Fiber Composites, Carbon Fiber Composites

1. INTRODUCTION

Wind turbine blades are designed to several major structural conditions, including tip deflection, strength and buckling during severe loading, as well as very high numbers of fatigue cycles during operation, varying between tension, compression and reversed tension-compression loads according to the particular loads spectrum for the turbine and wind conditions. The major static strength and stiffness properties depend primarily on fiber type, content, and orientation, following composite mechanics predictions widely available in the literature. The fatigue of composite laminates appropriate for wind turbine blades has been the topic of research studies for more than two decades; a general overview of this area can be found in reference (1). The findings of these studies are summarized in recent reports (2-4), and in two current public databases (5,6). Recent publications (7-11) are summarized here, with additional new data in several areas. The databases provide adequate constant amplitude fatigue data for the range of loading conditions necessary to define constant life diagrams and predict failure under spectrum loading (2,3,12). This requires testing for at least five or six load conditions, as described in detail in Reference 3 and 12. Precise laminate configurations for particular blades may not be included in the databases, but, in the absence of data for particular laminates, the fatigue trends may be assumed to apply in terms of strains.

Structural details such as ply drops used in thickness tapering, and special features such as sandwich panel close-outs and joints require separate attention. The fatigue response of structural details is typically dominated by crack initiation and growth in the matrix or adhesive (1,2).

Recent studies have focused on those materials issues which appear most likely to produce damage and failure for otherwise well designed and constructed blades (7-11):

1. tensile fatigue loading of glass fiber laminates,
2. compression static and fatigue loading of carbon fiber laminates,
3. ply delamination under a range of fatigue loading conditions, and
4. matrix cracking and transverse direction failure.

The succeeding sections describe the sensitivity to these issues of a range laminates of current interest in blades, in terms of fiber and matrix differences, fiber content and laminate construction, infused fabric architecture, processing, loading conditions, and ply drop geometry.

2. EXPERIMENTAL METHODS AND DATA REDUCTION

2.1 Materials A broad range of potential blade materials have been included in the course of this study, including E-glass, WindStrand™ and carbon fibers; polyester, vinyl ester and epoxy resins; a variety of laminate constructions and fiber contents, many stitched fabrics and several prepregs. Laminates were processed by resin transfer molding (RTM), vacuum assisted RTM (VARTM), SCRIMP™ infusion, and vacuum bag prepreg molding. The materials list covers most materials and process details. Other materials will be described in the foregoing, and further details may be found in the cited references.

Most of the materials are in the form of multidirectional laminates containing 0^o and $\pm45^o$ plies, with fiber volume fractions in the range of current infused or prepreg blades. Laminates used in blades typically vary from all unidirectional in some spars to a all $\pm45^o$ in some skins and webs. Testing experience both in this program (7,8) and European OPTIMAT program (3) has found that it is increasingly difficult, often impossible, to obtain gage-section fatigue failures under many testing conditions for laminates with strong fibers, high fiber contents and high fractions of 0^o plies. One outcome of this problem is a focus of the databases on laminates with significant $\pm45^o$ ply content. The testing philosophy is then to represent fatigue results in terms of strain rather than stress. Since all plies experience the same strains, other laminate configurations with a significant fraction of 0^o (main load direction) plies, including unidirectional, are assumed to fail at consistent strain-cycle conditions; this assumption is supported by test data in this study.

2.1.1 Materials List

1. DD Series . This is an early series of tests on E-glass/polyester laminates with 0^o Fabric A and $\pm45^o$ Fabric E (2).
   Lay-up and % 0^o-material: [0/±45/0]s; 72%-0^o
   Fiber volume fraction and thickness: both varied
   Matrix: polyester (CoRezyn 63-AX-051 with 1-2% MEKP)
   Process, cure and post-cure temperatures: VARTM, RT, 2 hours at 65^oC
   Laminate fabricated by: MSU
2. QQ1. E-glass/epoxy laminate based on 0^o Fabric B and $\pm45^o$ Fabric F
   Lay-up and % 0^o-material: $[\pm45/0_2]_S$, 64%-0^o
   Fiber volume fraction and thickness: 0.53 and 4.09 mm
   Matrix: epoxy (Vantico/Huntsman TDT 177-155)
   Process, cure, and post-cure temperatures: VARTM, RT, 6 hours at 70^oC
   Laminate fabricated by: MSU

3. QQ2. Same as QQ1 except lay-up $[\pm 45/0/\pm 45]_S$, $V_F = 0.52$, thickness = 3.96 mm.
4. QQ4. E-glass/epoxy laminate based on 0^o Fabric C and $\pm 45^o$ Fabric G
   Lay-up and % 0^o-material: $[\pm 45/0/\pm 45/0/\pm 45]$, 56%-$0^o$
   Fiber volume fraction and thickness: 0.57 and 4.03 mm
   Matrix: epoxy (Vantico/Huntsman TDT 177-155)
   Process, cure, and post-cure temperatures: VARTM, RT, 70^oC
   Laminate fabricated by: MSU
5. QQ4-L. Same as QQ4 except $V_f = 0.40$, thickness = 5.70 mm
6. QQ4-M. Same as QQ4 except $V_f = 0.46$, thickness = 4.85 mm, resin is epoxy SP Systems Prime 20LV with slow hardener, infused by VARTM at RT, post cured at 80^oC
7. E-LT-5500-EP. E-glass/epoxy laminate based on 0^o fabric D and $\pm 45^o$ Fabric G
   Lay-up and % 0^o material: $[\pm 45/0/\pm 45/0/\pm 45]$, 66%-$0^o$
   Fiber volume fraction and thickness: 0.55 and 4.59 mm
   Matrix: epoxy (Huntsman Araldite LY1564/hardener XB3485)
   Process, cure and post-cure temperature: Infusion (TPI SCRIMP^{TM}), 60^oC and 82^oC
   Fabricated by: TPI (Supplied by Global Energy Concepts (GEC)/BSDS Program (11))
8. E-LT-5500-VE. Same as E-LT-5500-EP except vinyl ester resin (Ashland Momentum 411-200), $V_f = 0.55$, thickness = 4.60 mm (supplied by GEC (11) as material EL-T-5500/VE)
9. TT. Similar to E-LT-5500-EP except fabricated at MSU by VARTM, resin is SP Prime 20LV with slow hardener, infused at RT, post cured at 80^oC, $V_f = 0.55$, thickness = 4.60 mm
10. TT1A. Same as material TT except ±45 fabric is Fabric F, resin is Vantico/Huntsman TDT 177-155, processed at RT by VARTM, post cured 6 hrs. at 70^oC, $V_f = 0.55$, thick = 4.37 mm
11. TT1AH. Same as material TT1A except $V_f = 0.63$, thickness = 3.98 mm
12. WS1. WindStrand^{TM} fiber/epoxy
   Lay-up and %-0^o material: $[\pm 45/0/\pm 45]$, 50%-0^o
   Fiber volume fraction and thickness: 0.61 and 2.56 mm
   Matrix: epoxy (MGS L135i/137i)
   Reinforcement (0 and ±45): WindStrand^{TM} 17-1200 SE2350M2 strands (2000 g/m^2) and DB1000 (same strands)
   Process, cure and post-cure temperature: vacuum infusion, 35^oC, 90^oC
   Laminate fabricated by: Owens Corning
13. WS2. Same as WS1 except $[\pm 45/0/\pm 45]_S$, $V_f = 0.60$, thickness = 5.19 mm
14. P2B. Prepreg hybrid carbon-glass (dispersed fibers in 0^o plies, fabric in ±45's)
   Lay-up and %-0^o material: $[\pm 45/0_4]_S$, 85%-0^o
   Fiber volume fraction and thickness: 0.55 and 2.75 mm
   Prepreg: 0^o-Newport NCT-307-D1-34-600 carbon; $\pm 45^o$-NB307-D1-7781-497A Glass
   Process and cure conditions: vacuum bag, 3 hrs. at 121^oC
   Laminate fabricated by: MSU
15. MMWK-C/G-EP. Infused carbon/glass triax hybrid, Fabric H
   Lay-up and %-0^o material: $[(45/0/-45)_4]$, 75%-0^o (by volume)
   Fiber volume fraction and thickness: 0.56 and 4.3 mm
   Matrix: epoxy (Jeffco 1401)
   Process, cure and post-cure temperature: TPI SCRIMP^{TM} infusion, 60^oC and 82^oC
   Laminate fabricated by: TPI (supplied by GEC/BSDS program (11))

16. CGD4E. VARTM carbon/glass hybrid, Fabrics A and I
Lay-up and %-0° material: [±45/0_3/±45], 76%-0°
Fiber volume fraction and thickness: 0.50 and 2.61 mm
Matrix: epoxy (SP Systems Prime 20)
Process, cure and post-cure temperature: VARTM, 20°C and 70°C
Laminate fabricated by: MSU

Table 1. Fabric specifications (from manufacturers).

	Manuf.	Designation	Fabric Weight, g/m^2	%0	%45	%90	%RM	%Stitching
A	Knytex	D155	527	99	0	0	0	1
B	Saertex	U14EU920-00940-T1300-100000	955	91	0	8	0	1
C	Saertex	S15EU980-01660-T1300-088000	1682	97	0	2	0	1
D	Vectorply	E-LT-5500	1875	92	0	6	0	2
E	Knytex	DB120	393	0	97	0	0	3
F	Saertex	VU-90079-00830-01270-000000	831	0	97	2	0	1
G	Knytex	DBM-1708	857	0	68	0	30	2
H	Saertex (11)	MMWK Triax glass/carbon/glass	970	69	31	0	0	NA
I	Toray	ACM-13-2 (300-48k-10C yarn)	600	100	0	0	0	NA
* Fabrics A-G are glass fiber, H is hybrid glass/carbon, and I is carbon. All listed percentages are by weight.								

2.2 Test Methods Test methods have been described in detail in References (7-11). Elastic modulus values were determined in tension at low strain (0.001-0.003 m/m) using an extensometer. Static strength values were determined either at low rates typical of test standards or at higher rates typical of fatigue tests (7), as noted for particular datasets. Typical tensile strength values are about 15% higher for the higher rate for glass fiber laminates (7). Typical test geometries for static and fatigue tests are given in Figure 1, with failed specimens shown in Figure 2. The short, rectangular specimens were used for tests involving compression loads, or as noted. Failure locations were usually adjacent to or inside the grips for rectangular specimens regardless of whether tabs were used (7). This testing problem has also been reported in other programs with similar materials (6). Tensile fatigue tests using the dog-bone geometries failed consistently in the gage section (8). Fatigue tests were run under load control, constant amplitude as illustrated for various minimum to maximum stress ratios, R, illustrated in Figure 3. The test frequency was typically below 10 Hz and specimen surfaces were air cooled with fans to avoid heating of more than a few °C (2). The frequency was also selected so as to approximately maintain a constant average load rate, increasing with decreasing maximum load (4). For tensile fatigue tests, the strains given are initial strains measured on the first few cycles. Strains for other R-value tests, using the short rectangular specimens shown, were determined from the stresses through the tensile modulus given in each case. In either event, the strains are lower than those which will accumulate during the fatigue lifetime (1-3, 5). A useful description of the effects of

the method of strain determination on strain based fatigue curves for several of the materials reported here is given in Reference (11).

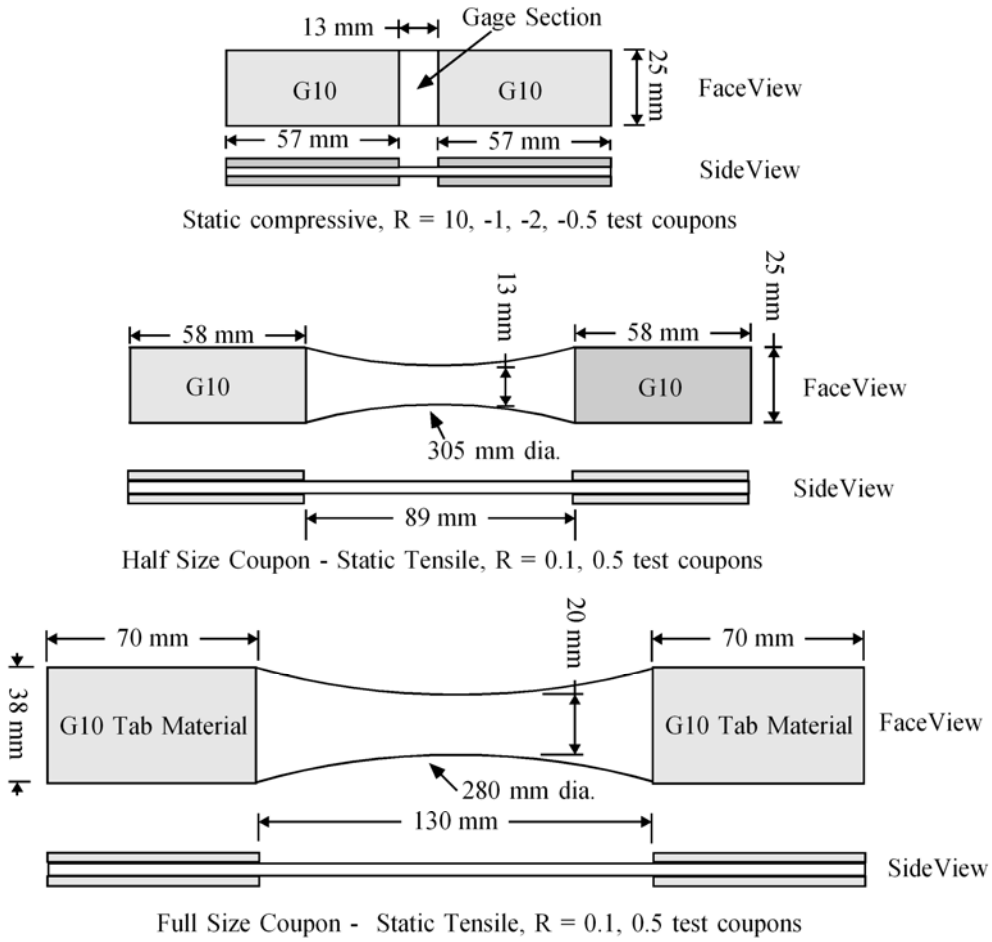

Figure 1. Rectangular (top) and Dog-bone Test Geometries: half (center) and full size (bottom) (7).

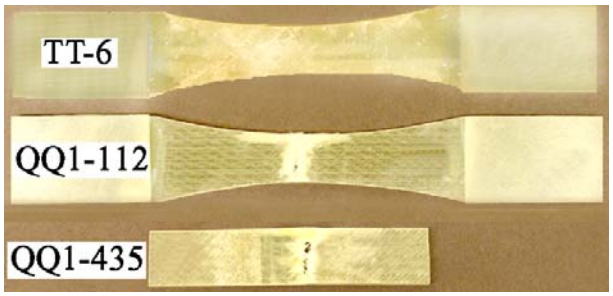

Figure 2. Failed fatigue dog-bone and rectangular specimens, showing grip-edge failure for a rectangular specimen (bottom) and gage section failure for a dog-bone specimen (7,8).

Delamination test methods for pure and mixed modes (I and II) used double cantilever beam (DCB), end notch flexure (ENF) and mixed mode bending (MMB) geometries described in

Reference 2. Thin and thick test coupons containing ply drops, shown in Figure 4, are described in more detail later (9).

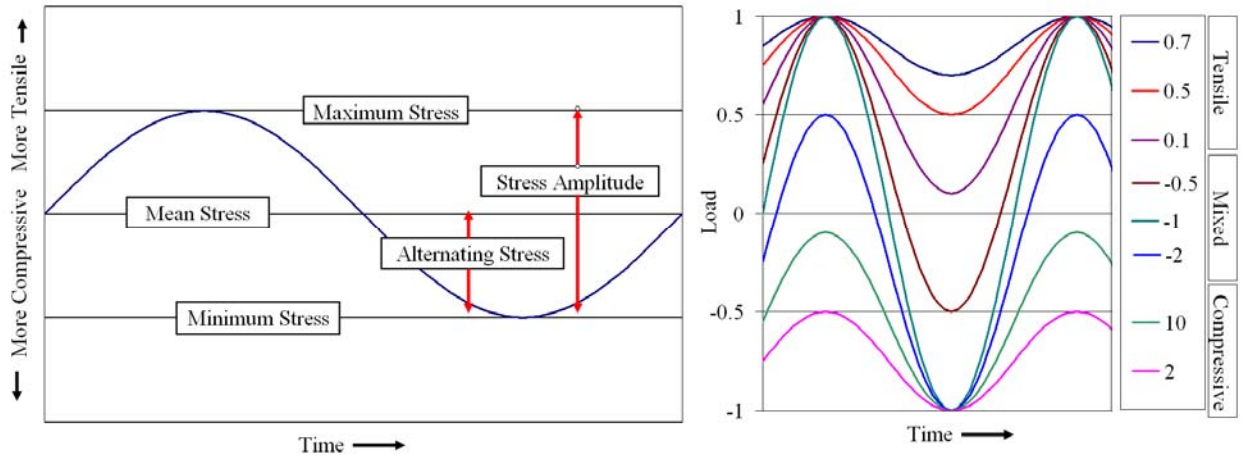

Figure 3. Load Waveforms Showing Definition of Terms (Left) and Illustration of R-values (Right, R-value = Minimum Stress/Maximum Stress) (7).

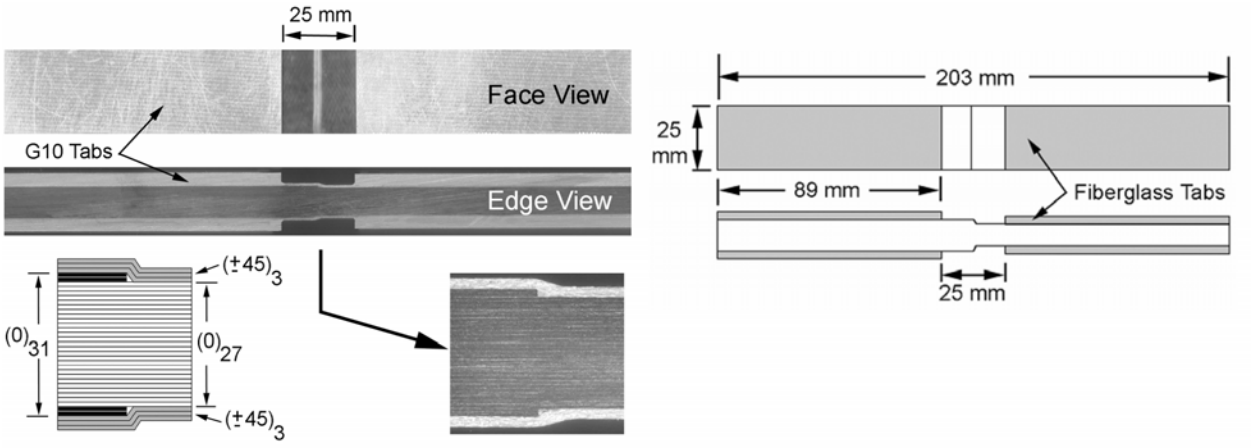

Figure 4. Typical coupon containing double 0^o ply drop at surface of 0^o ply stack; carbon prepreg 0° plies, glass prepreg $\pm 45^o$ plies (9).

2.3 Fatigue Models and Data Reduction Data reduction for fatigue tests includes least squares fitting of the fatigue trends with a power law model (Eq. 1) illustrated for a DD series material dataset in Figure 5, which compares the power law fit to exponential and three-parameter models. The power law provided a better fit to the fatigue data than the exponential model in most cases investigated (7); cases where the exponential model (Eq. 2) provided an improved fit includes delamination from ply drops, discussed later. The exponential model tends to better fit the low cycle and static data as shown, but the power law provides a better fit to the higher cycle data, and has also been shown to represent small impregnated glass strand data to 10^{10} cycles (2). The three-parameter model shown provides an improved fit to the overall dataset, but does not provide a consistent set of fitting parameters compared to the power law, and is inconvenient to manipulate (7). Most of the datasets in this study are fit by Eq. (1) to the fatigue data for cycles above about 10^3; the fits represent the mean lifetimes. The fits include static data for most carbon

laminates except material P2B, due to improved fits for the relatively less steep S-N curves. Other representations such as the 95/95 confidence limits for these datasets can be found elsewhere (7,12).

$$S = A\ N^B \qquad [1]$$

$$S = A - B \log N \qquad [2]$$

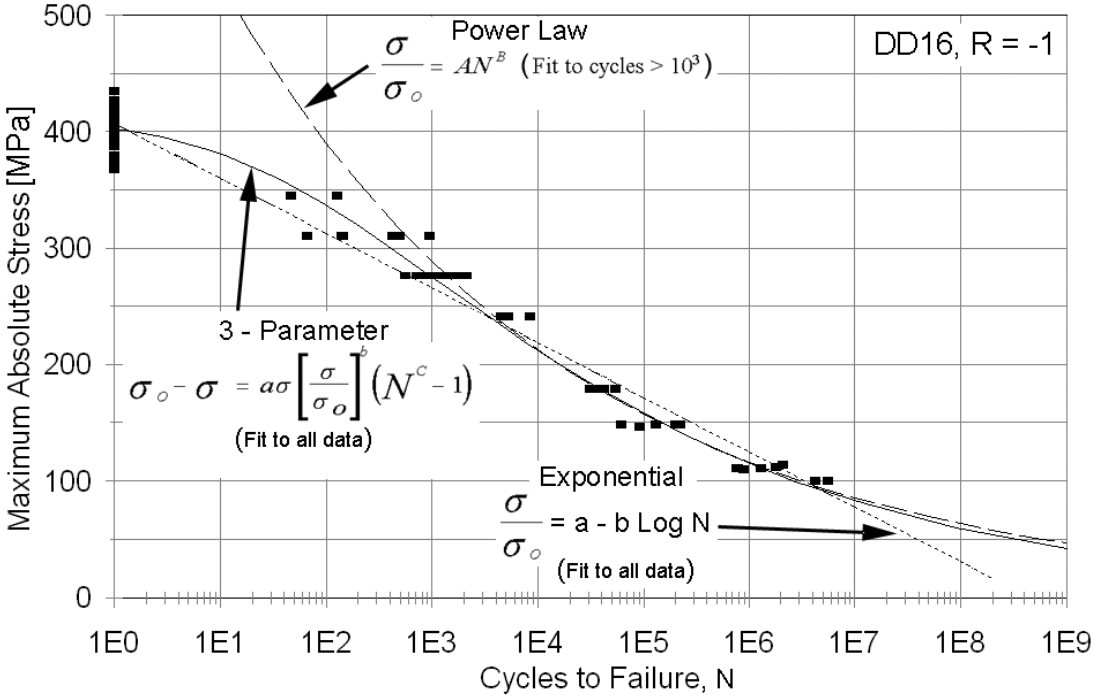

Figure 5. Material DD16, R = -1, S-N dataset with three curve fits, glass/polyester laminate (shown with static compressive strength) (7).

3. RESULTS AND DISCUSSION

3.1 Static Properties Laminate elastic modulus and ultimate strengths are listed in Tables 2 and 3. Since the laminates include differing contents of 0^o, 90^o, and $\pm 45^o$ material, the elastic modulus in the longitudinal direction of the 0^o plies, E_L, is given in Table 2 (taken from unidirectional laminates, adjusted proportionately to 53 % fiber; actual unidirectional laminates varied from 53 to 57 %). Tensile strength values are compared in Reference 7 (determined with DB specimens except for P2B, which used rectangular specimens) for both standard displacement rates, 0.02 mm/s, and also at a faster rate, 13 mm/s, representative of the displacement rate in fatigue. This approximately three orders of magnitude rate difference produces a 13-21% strength increase for the glass laminates at the high rate; rate effects are small for carbon (2% increase). Rate effects on static strength values should be considered carefully in using results such as S-N datasets and constant life diagrams. For example, while static data at the faster rate are generally used with these datasets in this study and in the DOE/MSU database (5) the slower, standard static strength testing rate is used in the OPTIMAT program (6). In this

paper the higher rate is used for static strength determination to be consistent with the fatigue rates. Compression tests used the rectangular specimen geometry with a gage length of 13 mm. Modulus values were determined in tension using slow load steps, over a strain range of 0.1 to 0.3%, with rectangular or BD specimens.

Glass fiber blade designs are often driven in part by deflection limits, so the modulus values are important. The different laminates, described earlier in detail, differ in the lay-up and 0^o ply content. The longitudinal modulus of the 0^o plies gives a more direct basis for comparison. The modulus values in Table 2 demonstrate the importance of fiber modulus; the great advantage of carbon fiber 0^o plies in material P2B is demonstrated in this Table, as is the improved longitudinal modulus of the WS1, with WindStrand™ glass fibers, compared with E-glass.

Table 2. Unidirectional longitudinal elastic modulus for several fabrics (normalized to a fiber volume fraction of 0.53).

Fabric or prepreg	Fiber	Matrix	0^O Ply Modulus, E_L, GPa
Fabric B	E-glass	Epoxy	42.5
Fabric D	E-glass	Epoxy	41.6
P2B, 0^o plies	Carbon	Epoxy	123
WS1, 0^o plies	Windstrand	Epoxy	48.3

3.2 Fatigue Results

3.2.1 Effects of Fiber Type Figure 6 compares the tensile stress and strain based fatigue resistance in tension (R = 0.1) and compression (R = 10), for four laminates representing three main fiber types, all with epoxy resins: E-glass (or Advantex™), QQ1 and E-LT- 5500-EP; WindStrand™, WS1 and WS2; and carbon hybrid (Grafil 34-600, 48k tow), P2B. The laminates have differing contents of 0^o plies relative to $\pm 45^o$ plies, slightly different fiber contents, and different processing, as defined in the materials list. Notable differences in fatigue performance are that the carbon hybrid is superior in terms of stress, and shows a much less steep fatigue curve compared to the glass fiber materials at R = 0.1 (tension). The compression fatigue curve for carbon is again less steep. Of the glass laminates, QQ1 is notably less tensile fatigue resistant, as discussed in the next section, and E-LT-5500-EP is less compression fatigue resistant. WindStrand™ is generally similar to the best of the E-glass laminates in each case, but slightly stronger in terms of stress, in tension. The aligned strand structure of the WindStrand™ WS1 laminates may be advantageous compared with stitched fabrics used for QQ1 and E-LT-5500 (8). By way of comparison, E-glass laminates MD2 in the European OPTIMAT program, fabricated by LM, show slightly lower failure strains in tension than E-LT-5500-EP, with a similar trend; these laminates were infused uni-fabric (0^o strands stitched to mat, Combimat 1250) as well as $\pm 45^o$ fabric (3).

The failure sequence for all of the laminates in tension started with matrix cracking in the $\pm 45^o$ plies, shown in Figure 7, as is commonly observed for most multidirectional polymer composites (13). The matrix damage can significantly reduce the modulus, increasing the strain in the constant stress amplitude tests (2,3,14). Matrix damage for the more tensile fatigue resistant

laminates like WS1 and E-LT-5500 was excessive prior to total failure (see Fig. 2, specimen TT-6). Compression fatigue failures were sudden, with little matrix cracking before total failure.

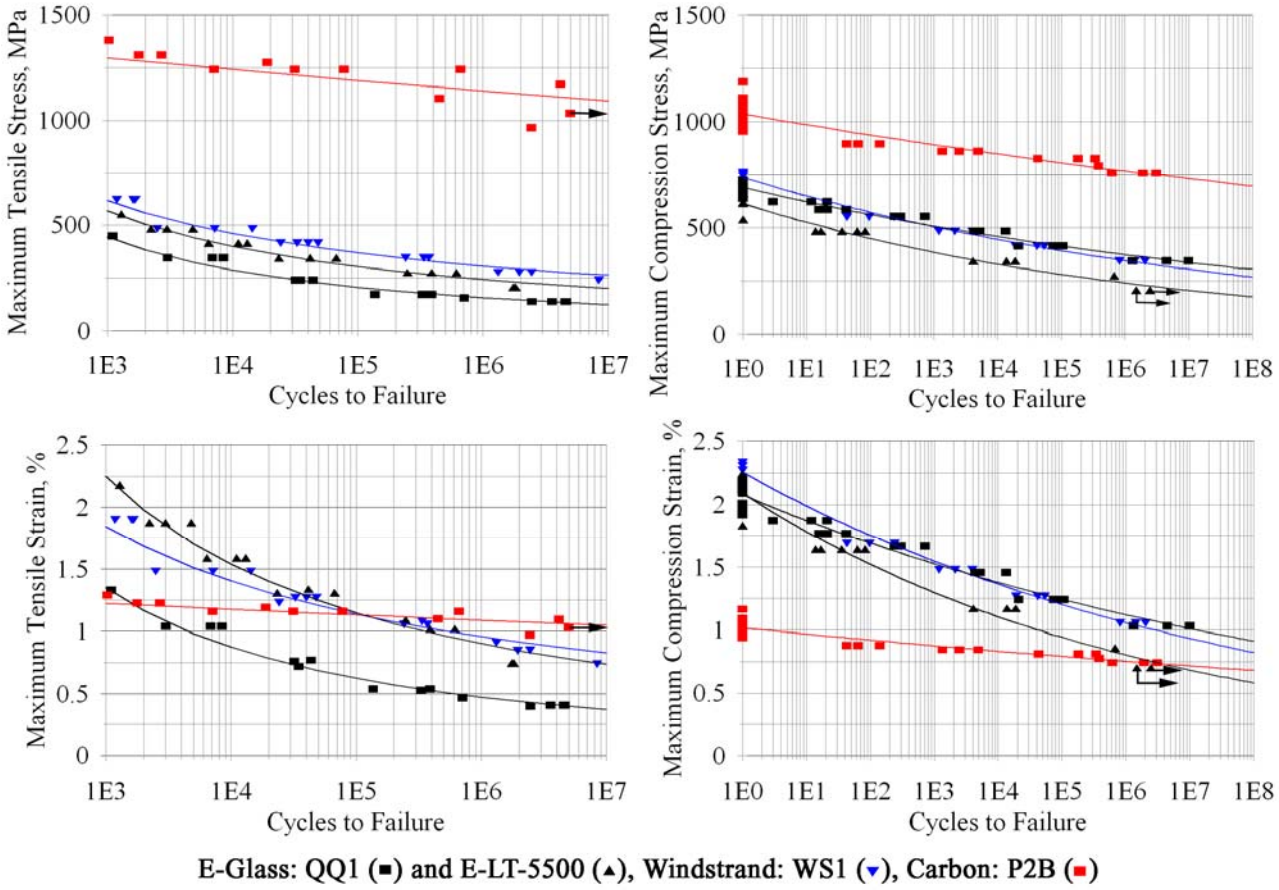

Figure 6. Fatigue comparison of multidirectional laminates based on E-glass (QQ1 and E-LT-5500), WindStrand™ (WS1) and carbon (P2B) fibers at similar fiber contents, in terms of stress (top) and strain (bottom), epoxy resins, R = 0.1 (left side) and R = 10 (right side).

3.2.2 Effects of Reinforcing Fabric and Process

3.2.2.1 E-glass Reinforcement Different materials based on different reinforcing fabrics (see the materials list) are compared in terms of the maximum tensile fatigue strain which can be withstood for a million cycles (Table 3), determined from the curve fits in Table 3. Other measures of fatigue resistance such as the exponents of the S-N fits in Table 3 would show consistent trends. Figure 8 shows a typical fabric, fabric A in Table 1, which contains relatively large inter-strand channels for resin flow. The results in Figure 9 for laminates based on various stitched E-glass fabrics show a marked difference in tensile fatigue resistance. (Note that many other commercial fabrics from different manufacturers are available, but were not included in this study.) The general trend of the results is clear for the DD Series laminates based on Fabric A. As the fiber content increases (as determined by the mold opening in the VARTM process with hard molds on both sides), the fatigue resistance as represented by the million cycle strain decreases rapidly above about 40% fiber by volume. The strain capacity at higher fiber contents

Table 3. Average static data and fatigue fit parameters.

Material	V_f %	R	Static* Strength MPa	Ultimate* Strain, %	Elastic Modulus GPa	10^6 cycle strain, %	Eq. (1) Mean Fit Parameters			
							Strain		Stress	
							A	B	A	B
QQ1	53	10	-687	-2.05	33.1	-1.12	2.078	-0.045	690	-0.045
		-2				-0.92	2.111	-0.060	698	-0.060
		-1				0.43	2.557	-0.129	931	-0.138
		-0.5				0.51	3.535	-0.141	1173	-0.141
		0.1	843	2.56		0.47	4.032	-0.156	1328	-0.156
		0.5				0.71	3.426	-0.114	1359	-0.131
QQ1T	53	10	-274	-1.59	17.1	-0.76	1.380	-0.043	281	-0.104
		-2				-0.38	1.628	-0.104	281	-0.104
		-1				0.20	1.014	-0.117	175	-0.117
		-0.5				0.21	0.961	-0.109	166	-0.109
		0.1				0.28	0.841	-0.081	145	-0.081
		0.5	149	0.86		0.23	0.896	-0.098	155	-0.071
		0.7				0.42	0.814	-0.048	141	-0.048
QQ2	52	0.1	552	2.50	23.3	0.63	3.731	-0.129	735	-0.122
QQ4	57	0.1	986	3.10	31.8	0.59	3.589	-0.131	1048	-0.126
		10	-601	-1.89		-0.82	2.331	-0.076	742	-0.076
QQ4L	40	0.1	673	3.13	21.5	1.15	4.474	-0.098	939	-0.098
QQ4M	46	0.1	790	3.09	25.6	0.76	5.038	-0.137	1071	-0.128
E-LT-5500-EP	55	0.1	837	3.36	29.4	0.89	5.322	-0.130	1264	-0.121
		10	-552	-1.88		-0.80	2.138	-0.071	623	-0.069
E-LT-5500-VE	55	0.1	809	2.47	30.5	0.72	4.624	-0.134	1146	-0.138
		10	-670	-2.09		-0.94	2.527	-0.071	811	-0.071
TT	55	0.1	858	2.96	29.0	0.84	5.309	-0.134	1523	-0.133
TT1A	55	0.1	899	3.24	27.7	0.97	3.965	-0.102	1176	-0.109
TT1AH	63	0.1	930	2.95	31.5	0.63	3.694	-0.128	1163	-0.130
WS1	61	0.1	865	2.72	32.6	0.98	2.902	-0.079	932	-0.078
WS2	60	10	-755	-2.31	32.2	-1.06	2.260	-0.055	737	-0.055
P2B	54	10	-1047	-1.03	101	-0.76	0.946	-0.015	964	-0.015
		-2				-0.58	1.089	-0.045	1114	-0.046
		-1				0.60	1.017	-0.038	1038	-0.038
		-0.5	1546	1.43		0.72	0.909	-0.017	972	-0.017
		0.1				1.09	1.424	-0.019	1549	-0.023
		0.5				1.19	1.315	-0.007	1406	-0.007
MMWK C/G-EP	55	10	-873	-1.37	67.2	-0.70	1.377	-0.049	874	-0.041
CGD4E	43	10	-684	-0.81	86.2	-0.53	0.781	-0.029	673	-0.029

*Positive stress and strain = tensile. Negative stress and strain = compressive. ** Curve fits do not include static data except for materials MMWK-C/G-EP and CGD4E.

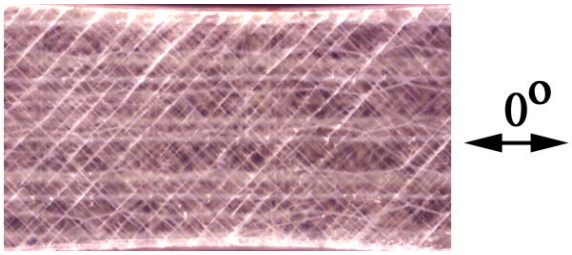

Figure 7. Cracking in ±45^{O} plies of material QQ2 specimen prior to total failure (7).

drops to less than half the value at lower fiber contents. At the other extreme, materials based on fabric D retain good tensile fatigue resistance to above 55% fiber by volume, then drop above 60% fiber; these results approach those for prepreg and aligned strand laminates (2,8). Fabric C in the QQ4 series laminates is very similar in construction and weight to fabric D, but shows a transition to lower fatigue resistance at much lower fiber contents, close to fabric A. The lighter weight but otherwise similar fabric B (materials QQ1 and QQ2) shows even lower fatigue strains than fabric C.

The differences in materials such as QQ1 and QQ4 (fabrics B and C) and TT and E-LT-5500 (fabric D) at similar fiber contents and overall fabric specifications (Figure 9) is pervasive over entire panels and for different batches, with different processors. No individual fatigue test results (Figure 6) for the more fatigue sensitive materials approach the worst performing specimens from the less fatigue sensitive materials at the same strain level. This despite similar static properties. Thus, the increase in fatigue sensitivity is not due to some form of occasional flaw, but is inherent in the gage section of every test specimen. The differences observed between these fabrics (8) relates primarily to the extent of distortion (Figure 10) and compaction (Figure 11) in the strands when the fiber content is increased. The main advantage of fabric D appears to be in the stitching details rather than the general fabric specifications (Table 1).

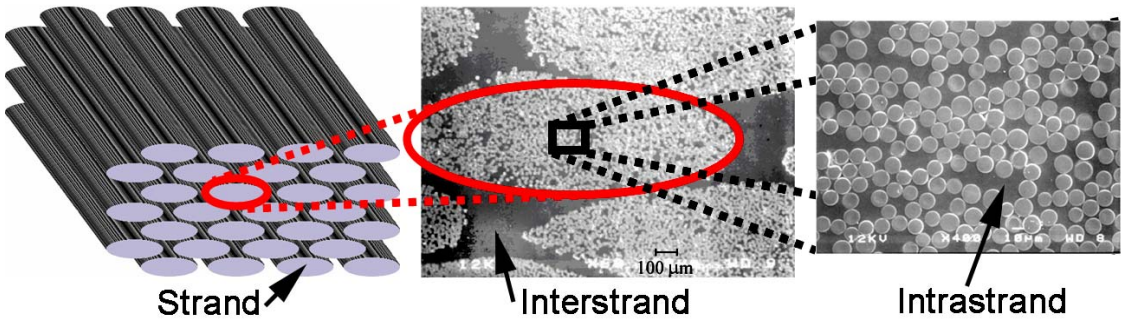

Figure 8. Exploded view of D155 Fabric A composite showing inter-strand channels and intra-strand structure (8).

As discussed elsewhere (8), fabrics C and D are very similar in construction, given in Table 1. In cross-section, these fabrics are densely packed compared with fabric A due to their rectangular strand cross-sections and large strands, with small inter-strand areas (Figure 8). The fiber content as a function of mold pressure has been determined (Figure 12) for Fabrics A, C, and D, following methods described elsewhere (2). Fabrics C and D are very similar in terms of the

fiber content reached as a function of mold pressure, while Fabric A is reaches much lower fiber contents for the same pressure. At low pressure conditions like 10-20 kPa, fabric A fiber content is around 40%, while fabrics C and D are around 55% fiber by volume; these ranges are typical of hand lay-up vs. infusion processes for which the fabrics are apparently designed. Transitions to poor fatigue resistance occur as the fiber content is raised above the low pressure range for Fabrics A and D, but at a lower fiber content for fabric C.

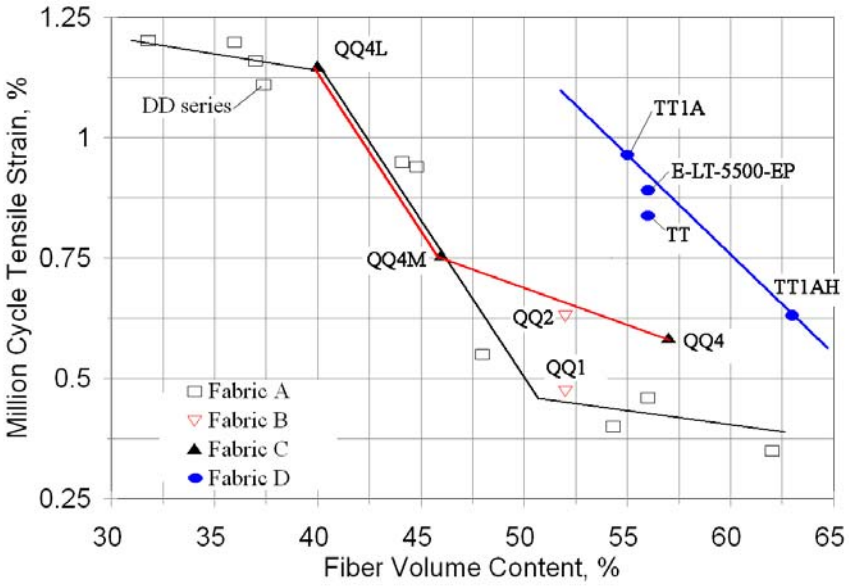

Figure 9. Million cycle strain vs. fiber volume content for various infused materials showing transitions to reduced fatigue resistance as a function of 0^o fabric, R = 0.1 (8).

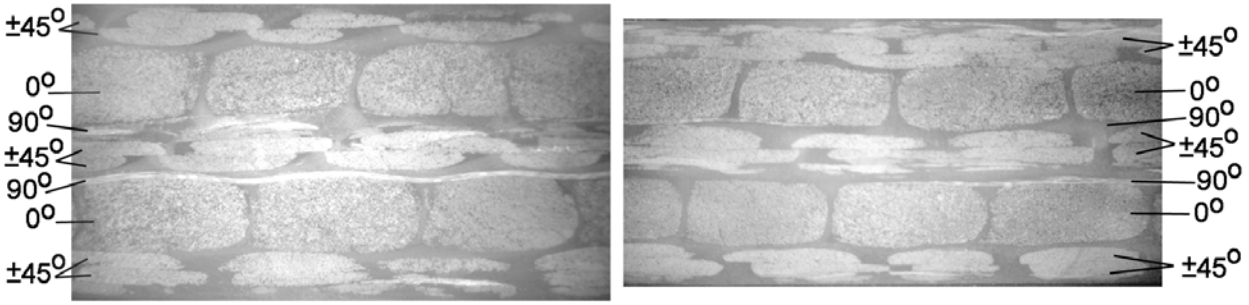

Figure 10. Comparison of cross-section views of laminates QQ4 (fabric C), and TT (fabric D) (8).

3.2.2.2 Carbon Reinforcement Carbon fiber reinforced laminates for wind blades are most limited by compressive strength and ultimate strain (2, 10). The presence of even minor amounts of fiber misalignment has been shown to reduce static and fatigue properties significantly (15). Maximum compressive properties are obtained with strands which have the least misalignment, generally unidirectional prepreg 0^o plies; poorest properties have been found with woven fabrics, particularly with large tows. Figure 13 compares the compressive static and fatigue properties for three laminates (see materials list for details): P2B, relatively thick (0.3 mm) prepreg with

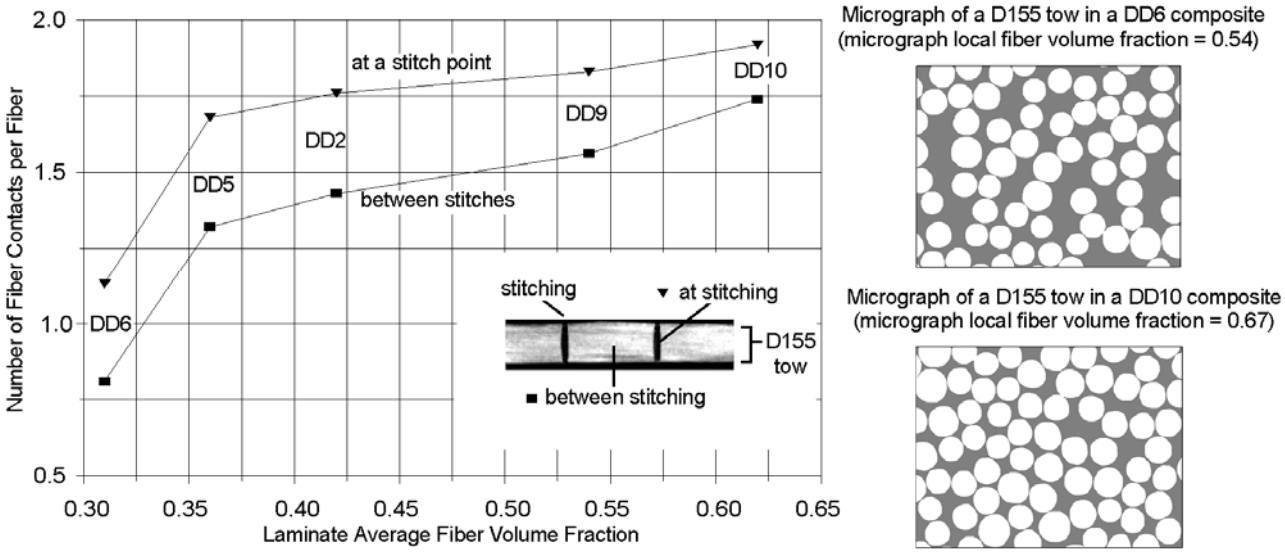

Figure 11. Number of contacts per fiber from neighboring fibers along stitch line and between stitch lines vs. average laminate fiber volume fraction, also showing micrographs (bottom) for intra-strand fiber packing, selected DD-series laminates (2).

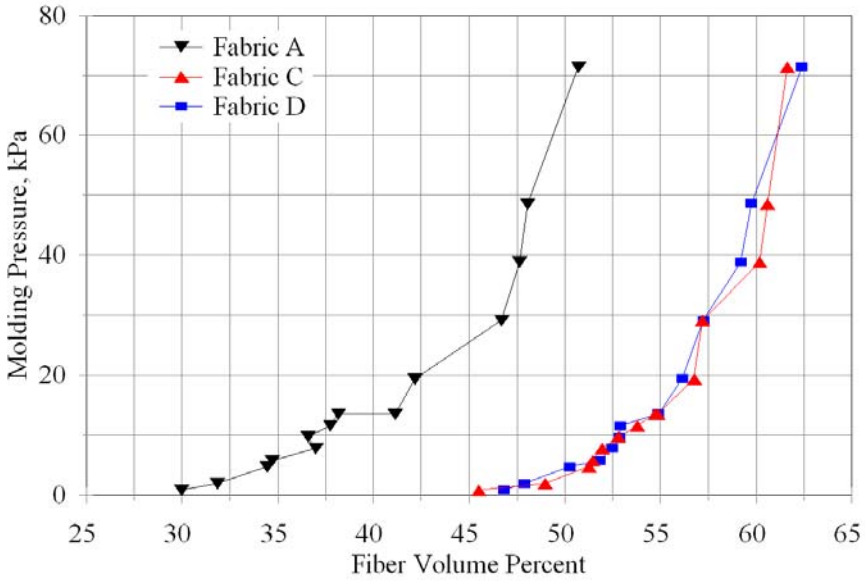

Figure 12. Mold pressure vs. fiber content for fabrics A, C, and D, measured for fully wet-out [0_2] laminates (8).

unidirectional carbon fiber 0° plies; MMWK C/G-EP, infused triaxial fabric H with +45° and -45° E-glass plies sandwiching 0° carbon strands; and CGD4, VARTM processed 0° stitched carbon fabric with E-glass ±45° plies. The P2B laminate gave properties typical of other large tow prepregs (2, 11). The CGD4 laminate was among the best stitched or bonded carbon fabrics tested (2), but inferior to the prepreg, apparently due to slight misalignment in the fabric strands. The MMWK- C/G-EP laminate properties were at least equivalent to various prepregs tested in this program, with very straight strands held in place by the 45's; this fabric contains about 25 %

off-axis material by volume which reduces the strength and modulus values relative to unidirectional carbon laminates (11) (Tables 1-3).

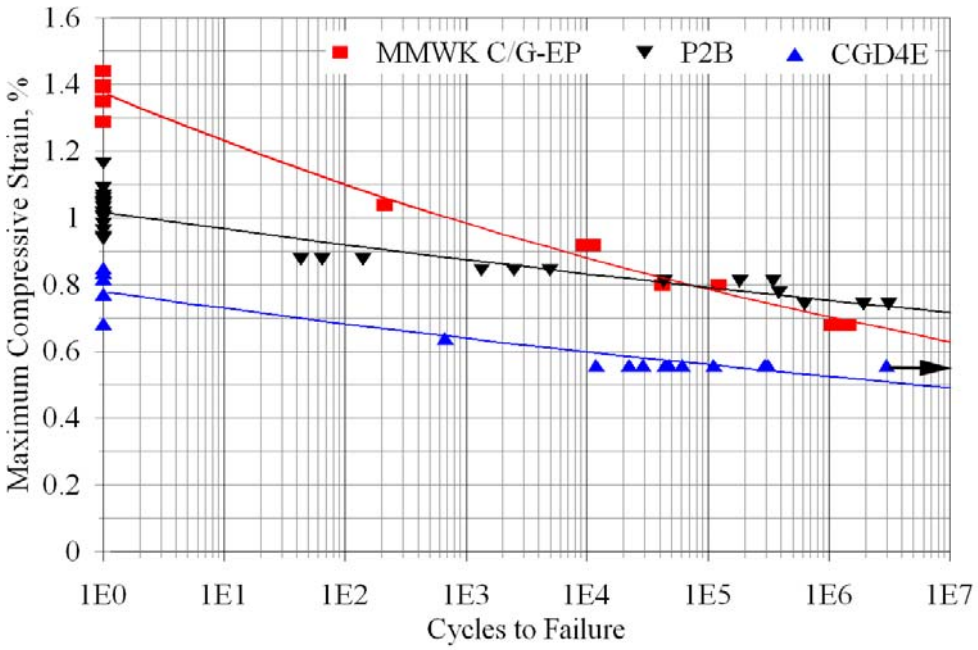

Figure 13. Comparison of compressive fatigue resistance of hybrid laminates with carbon 0^o plies and E-glass $\pm 45^o$ plies: materials P2B (prepreg); MMWK C/G-EP (infused stitched hybrid triaxial fabric); and CGD4E (VARTM stitched fabrics), R = 10.

3.2.3 Effects of R-value Figure 14 gives a full dataset for E-glass laminate QQ1 at six R-values. Fit parameters can be found in Table 3. It should be noted that only the R = 0.1 specimens failed consistently in the gage section (Fig. 2). This laminate is more sensitive to tensile fatigue in this fiber content range than those based on Fabric D, as noted earlier, but is typical of many laminates using stitched and woven fabrics (2). The loading conditions with the greatest tensile amplitude, R = 0.1, -0.5 and -1 fail at the lowest maximum strains at high cycles. As indicated in Figure 6(a), laminate E-LT-5500 and other laminates based on Fabric D show significantly higher tensile fatigue strains compared to QQ1. The next section describes combining these data into a constant life diagram (CLD). Data of this type for glass/epoxy (3) and polyester (2) have also been reported, the latter for thirteen R-values.

Much less steep fatigue trends are demonstrated for carbon hybrid laminate P2B in figure 15 at each R-value. Very similar trends at the same R-values have been reported for the infused triaxial hybrid fabric laminate MMWK C/G-EP. Mean lifetime fits for carbon materials include the static data, since the goodness of fit is improved (10).

3.2.4 Constant Life Diagrams

Constant life diagrams, CLD's, have been prepared for materials QQ1 (glass/epoxy) and P2B (hybrid carbon/glass with carbon 0^o plies), in the axial and transverse directions. The full dataset including mean and 95/95 CLD's is available from References 7 and 10, and only selected results are given here. The CLD's are constructed from the fit parameters in Table 3. Figures 16

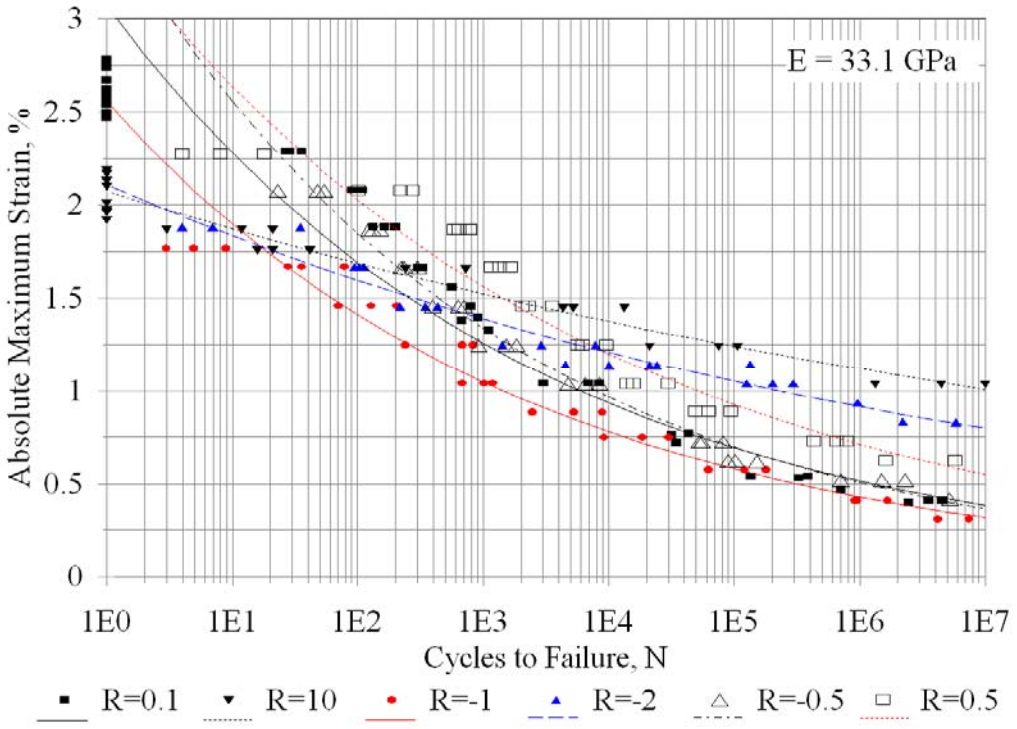

Figure 14. Effect of loading conditions (R-value) on fatigue strain vs. lifetime for E-glass/epoxy laminate (QQ1).

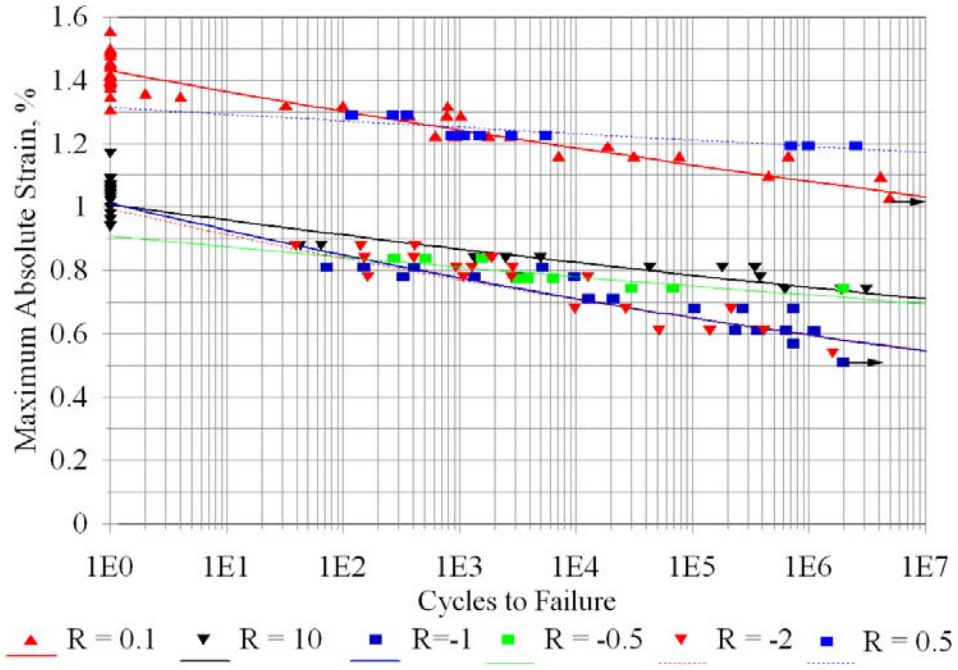

Figure 15. Maximum Absolute Strain to Failure Fatigue Data for [±45/0_8/±45] P2B Laminate, R=0.1, 10 and -1 (9).

and 17 compare the mean CLD's for laminates QQ1and P2B based on stress and strain, respectively. As noted above, QQ1 material shows poor tensile fatigue resistance compared to other current E-glass/epoxy laminates, including both those based on Fabric D, laminate DD16 (at lower fiber content) (2) and results reported for material MD2 in the European OPTIMAT program at similar fiber content to QQ1 (3). The transition from compression to tensile failure modes around R = -1 is particularly severe for this material at high cycles. The carbon hybrid laminate, P2B, is much stronger than QQ1 in both static and fatigue tests (Fig. 16). On the basis of strains (Figure 17) the order is reversed for most conditions, except in the tension quadrant at high cycles. Even on a strain basis, however, the carbon fatigue curves are much less steep (Figures 14 and 15), and carbon dominated blade designs may be driven by static rather than fatigue properties, particularly ultimate compressive strain (15).

The transverse direction mean stress CLD for material QQ1 is given in Figure 18, with strains calculated from the stresses through the transverse modulus (7). These 0^o dominated laminates are relatively weak in the transverse direction (Table 3) as expected, particularly in tension. The CLD shows much better performance in the compressive than the tensile quadrant. A similar transverse direction CLD is reported elsewhere (7) for material P2B. Comparison of the axial and transverse diagrams for material QQ1 and P2B indicate the general trend that matrix cracking for R-values containing tension occurs at lower strains than does fiber dominated failure, in this case for transverse loading. Laminates loaded in the axial direction will generally develop matrix cracking in off-axis plies prior to total failure for these conditions, and this stable damage can become severe for materials which are more resistant to fiber failure, like those based on fabric D, as discussed earlier (2,4).

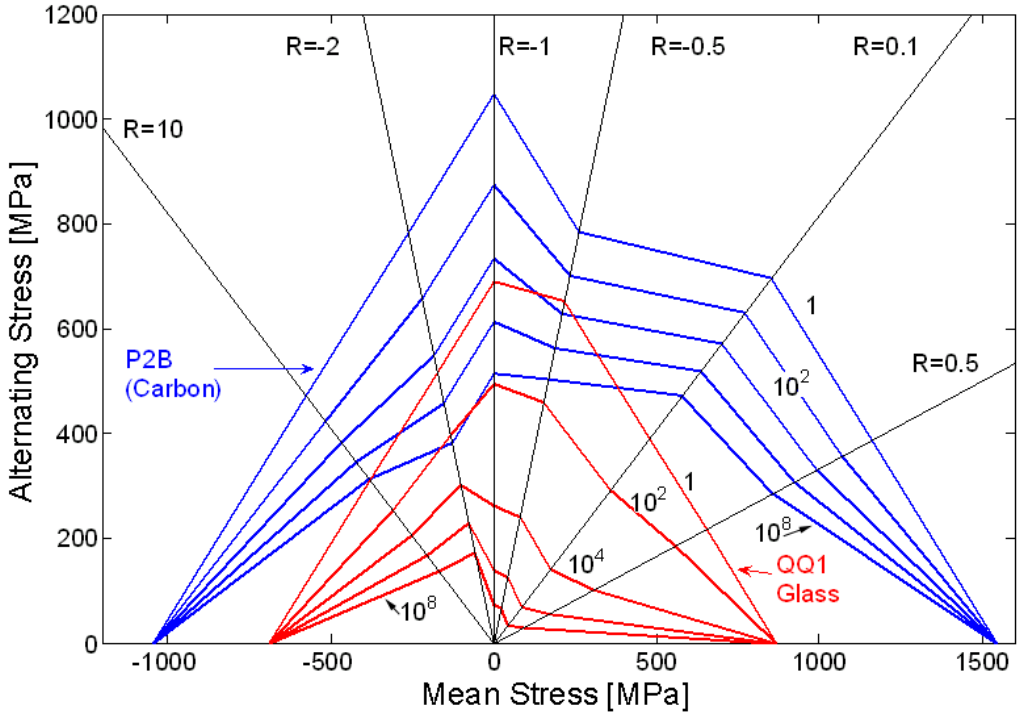

Figure 16. Comparison of materials QQ1 (E-Glass) and P2B (carbon 0^o plies), axial direction, mean stress constant life diagram (7).

3.3 Matrix Effects on Fatigue and Delamination Resistance Epoxy, vinyl ester and polyester resins have been investigated in the context of this class of materials. Aside from processing variations, little effect was seen with glass laminates in the main fiber direction (2,4). Vinyl esters were found to give slightly lower static and fatigue strengths with carbon fibers (2). The main differences for the three resin types were found in the compressive, transverse, and shear properties for hot/wet conditioning and testing (2). Ortho-polyesters and epoxies with lower post cure temperatures were found to degrade significantly, primarily as the test temperature approached the post cure temperature for infusion epoxies. Vinyl esters and iso-polyesters were particularly insensitive to hot/wet conditions (2). More recent tests on infused epoxy and vinyl ester laminates has shown somewhat lower tensile fatigue resistance for the vinyl ester, but the opposite was observed in compression; the properties were similar in reversed loading (11).

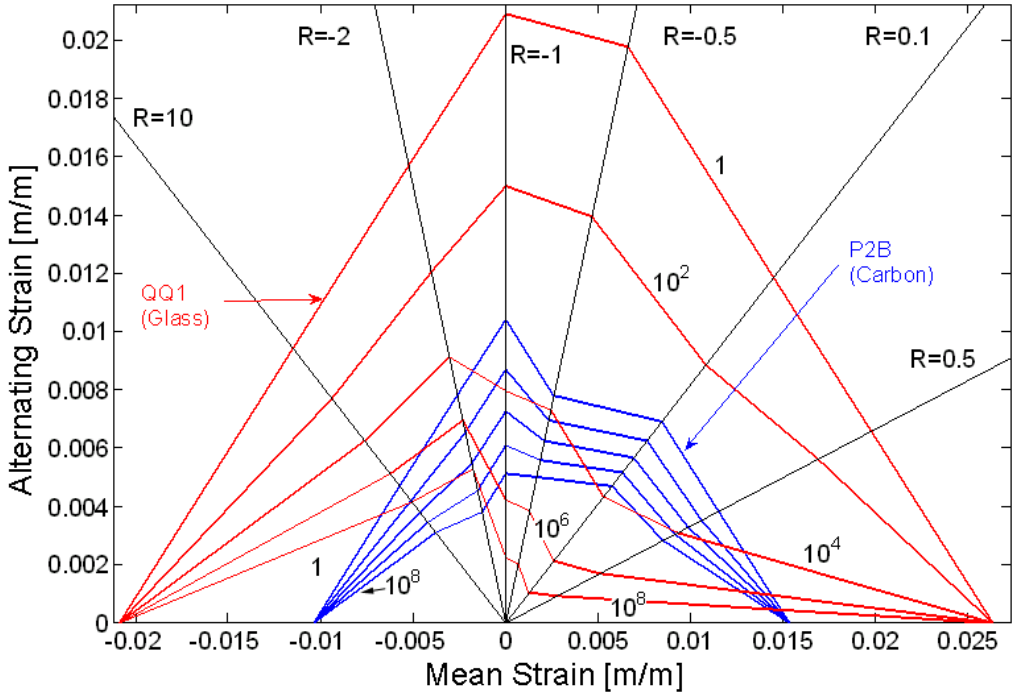

Figure 17. Comparison of materials QQ1 (E-Glass) and P2B (carbon 0^o plies), axial direction, mean strain constant life diagram (7).

The resistance to delamination between plies in typical structural details is known to be dominated by the resin toughness, and so is sensitive to the type of resin (2). Tests can be run in Mode I (crack opening), Mode II (shear) or Mode III (tearing), or combinations of these (2). Most structural details experience a combination of Modes I and II, as explored for ply-drops in the next section. Test results, including environmental effects, have been reported (2) for laminates of the type discussed above. Figure 19 presents mixed Mode I and II data for the three resin types (SP Systems Prime 20 epoxy, Derakane 411-350 vinyl ester, and CoRezyn 75-AQ-010 iso-polyester). The comparison at low fiber content for fabric A shows significantly higher delamination resistance for epoxy than for vinyl ester, with polyester the lowest; the results are consistent over the entire range of modes, and are in the expected order. The same epoxy was tested with fabric D at the higher fiber content shown, and gave somewhat lower toughness than at the lower fiber content, a trend which is expected as the amount of resin in the inter-ply region

is reduced (2). The general trend of the data in Figure 19 with mode mixity is consistent with the model of Reeder (16) for relatively brittle resins. Results for skin-stiffener structural details show a trend for different resins which is consistent with delamination test results (2,17). Thus, data such as those in Figure 19 are generally consistent with structural integrity observations. The delamination tests can also be run in fatigue, to obtain fatigue crack growth trends, but results for this group of materials are only available for the polyester resin (14) in pure modes. The section which follows explores what is usually mixed mode delamination at ply drops used in thickness tapering.

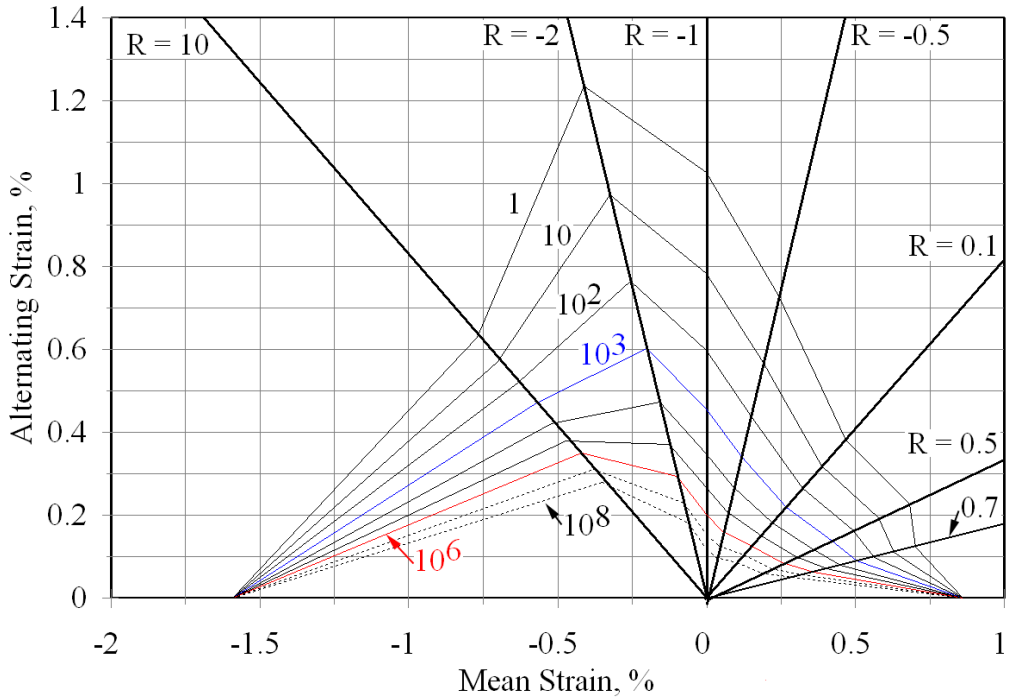

Figure 18. Transverse direction mean strain constant life diagram for material QQ1.

3.4 Ply Drop Delamination Ply drops are the main approach used to taper the thickness in composite structures like wind blades; an aerospace analog which has received attention in the literature is flex beams for helicopter blades (18). The study summarized here has been reported in more detail elsewhere (9, 10). Using test specimens similar to that shown in Figure 4, the effects of ply drop thickness, position, and overall laminate thickness have been explored under various loading conditions for stacks of 0^o plies with $\pm 45^o$ plies on the outside. In actual blades, a series of such ply drops is included in areas like spars to accomplish thickness tapering. The same resin and curing was used throughout the study with glass and carbon unidirectional plies and woven glass $\pm 45^o$ plies; detailed fabrication and testing procedures are given elsewhere (9,10). Testing concentrated on establishing the strain levels under fatigue loading for delamination and/or gross failure at ply drops. While fracture mechanics based methodology may be applied in studies to predict delamination growth (17), the most direct data for material selection and design of wind turbine blades are in the form of stress and strain levels to produce significant delamination, which can be used with traditional design and analysis methods. Interpretation of the experimental results and extension to other cases is provided by an on-going

finite element analysis of several of the cases, based on idealized geometries and interlaminar fracture mechanics (10).

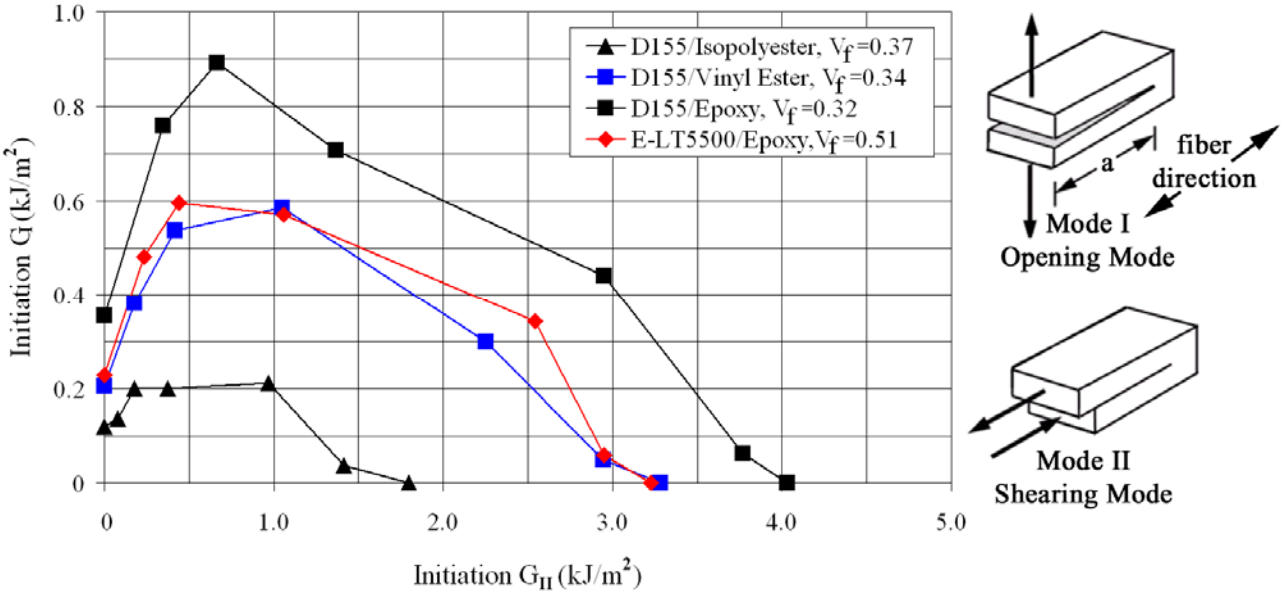

Figure 19. Mixed mode delamination resistance for two E-Glass fabrics with three resins .

Ply properties used in the finite element analysis are given for each prepreg in Table 4, along with pure Mode I and II delamination resistance. Compressive stress-strain curves were generated from specimens without ply drops to obtain modulus values used to calculate strains from the stress determined in the tests (10). All stresses and strains in the results represent the thin side of the ply drop specimens.

To minimize testing problems, a series of relatively thin laminates, on the order of three to four millimeters thick, was tested both with and without ply drops under tensile, compressive, and reversed loading. The results were then compared with data for relatively thick laminates more representative of blades for selected geometries under compressive loading (which could take advantage of end loading to avoid grip failures). The ply configuration for the thin laminates was $(\pm 45/0_9/\pm 45)$, with additional plies added for half of the coupon length in the case of ply drops. As noted earlier, the 0^o plies contained carbon fibers, while the $\pm 45^o$ plies contained glass fibers.

S-N fatigue data for coupons without ply drops were given in Figure 15 for this material system, for the similar ply configuration $[\pm 45/0_8/\pm 45]$ with the three R-values. The results for the thin laminates containing double ply drops, $[\pm 45/0_2{*}/0_9/0_2{*}/\pm 45]$, where the $0_2{*}$ plies are dropped at mid-length, are given in Figure 20 (corresponding stress based data can be found in References 9 and 10 for each case). The two double ply drops (total thickness dropped of 0.6 mm) reduce the static strengths by approximately 45% in tension and 42% in compression. The effects of ply drops on the fatigue life are significant, producing steeper S-N curves than for the control trend lines shown. Failure is taken as the growth of a large (6 mm long) delamination from the ply drop location, or else simultaneous delamination and separation. Delamination is a matrix failure mode which follows a steeper S-N trend than do control laminates which are more fiber dominated (2). Maximum strain levels for 10^6 cycles are below 0.3% for the laminates with double ply drops, compared with 0.6% to 1.0% for the control material, depending on R-value.

As with the control material, reversed loading is most severe. It is noteworthy that all three loading conditions produce delamination at the ply drop site in a similar strain range. Figure 21 is a photograph of a delamination crack growing from a ply drop with a typical pore at its tip; no significant difference could be determined between specimens with and without an obvious pore.

The delamination in Figure 21 is a single crack separating the dropped plies and outside ±45's from the remainder of the laminate. This pattern was observed for all coupons having ply drops at the outside of the 0^O-stack, including the thick laminates, whereas interior ply drops often showed two cracks, one growing on each side of the dropped plies. Finite element results showed that for this geometry, delamination is dominated by the Mode II, or shear component, as discussed below. Mode II has a similar G_{II} under tension and compression, but with the shear direction reversed, while reverse loading (R = -1) has twice the shear amplitude at the same maximum load, consistent with Figures 20. Damage was also observed in the ±45 plies in the taper area which has been shown to affect the G values (10).

Table 4. Ply properties and delamination resistance in material principle directions for E - glass and carbon prepregs (static longitudinal, transverse, simulated shear and delamination resistance).

	lay-up	V_F %	Elastic Constants				Delamination Resistance*		
			E_L GPa	E_T GPa	υ_{LT}	G_{LT} GPa	lay-up	G_{IC} (J/m^2)	G_{IIC} (J/m^2)
NB307-D1 7781 497A glass	0/90	39	19.2	19.2	0.13	3.95	----	----	----
NCT307-D1-34-600 carbon	$[0]_{10}$	53	123	8.20	0.31	4.71	$[0]_{20}$	364 (62)	1829 (87)
NCT307-D1-E300 glass	$[0]_{10}$	47	35.5	8.33	0.33	4.12	$[0]_{20}$	365 (37)	2306 (188)
* 13 to 14 tests, Brackets indicate standard deviation.									

The thin laminate data indicate a strong sensitivity to fatigue for all R-values. Thicker laminates were tested in compression, where direct end loading can be added to the shear loading through the tabs (Fig. 4). A comparison of thin and thick laminates in Figure 22 indicates very similar fatigue strains for the same double ply drop at each surface, with the thick laminate fatigue strains approaching 0.2% maximum compressive strain at high cycles. The effects of ply drop position through the thickness is not great, as shown in Figure 23. Figure 24 provides a comparison of the internal ply drop geometry with E-glass vs. carbon 0^o plies: on a strain basis, the carbon delaminates at much higher strains than does the glass, while carbon delaminates at somewhat higher stresses. Additional results reported in References 9 and 10 for other ply drop positions and numbers of dropped plies, for both glass and carbon, show similar trends, as do infused laminates with the hybrid triax fabric H (11).

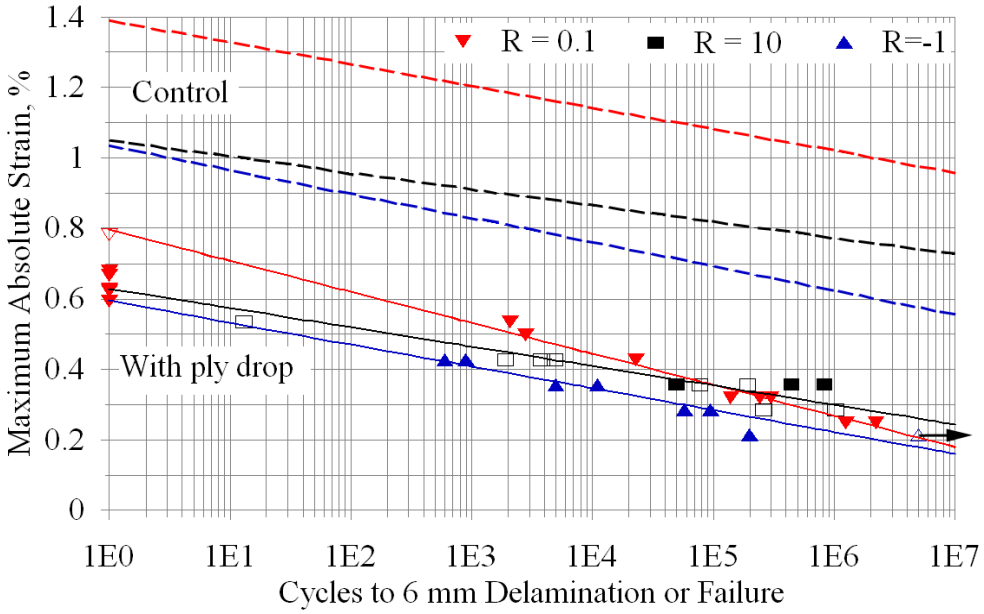

Figure 20. Maximum absolute strain versus cycles to failure (open symbols) and/or delamination (closed symbols) for thin laminates with double ply drops [±45/0_2*/0_9/0_2*/±45], R=0.1, 10 and -1, comparison with (dashed) trend lines for control laminates in Fig. 15 (0° plies are carbon, ±45° plies are glass) (9, 10).

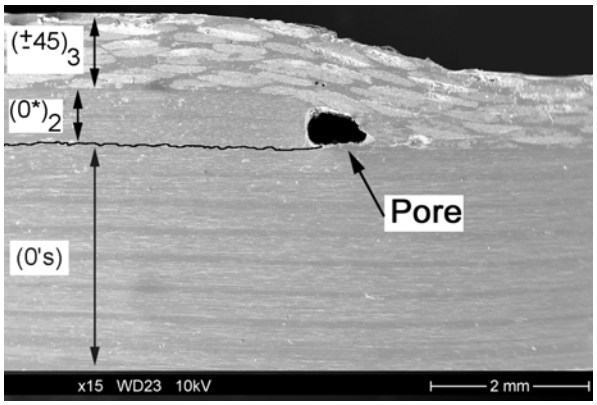

Figure 21. Photograph of delamination crack growing from pore ahead of double ply drop (see fig. 4), carbon 0^o plies, compression fatigue (crack path enhanced) (9, 10).

Variations in G_I and G_{II} have been determined by finite element analysis for a broad range of ply-drop, ply joint and material transitions, as a function of delamination crack length, for these materials in Reference 10, with limited cases reported in Reference 9. Figure 25 compares the forward shear, G_{II}, values for glass and carbon 0^o plies as a function of crack length at a thin side far-field static strain of 0.5%. (The model assumes equal crack lengths, which was not generally observed experimentally, and the results are given for the total of the G-values at each crack tip.) The results in Figure 25 help explain the various experimental observations, where carbon was much more prone to delamination than glass; the G_{II} values driving crack growth are over three

times as high for carbon as for glass at the same far-field strain. Compared to the critical Mode II G_{IIc} values in Table 1, the carbon is at about half the critical value of 1829 J/m^2, while the glass is much lower. While the finite element results are for static loads, the values are consistent with the fatigue curves in Figure 13 at the same strain level of 0.5%. Most ply drop geometries include a combination of Modes I and II, so interpretation requires a mixed mode criterion as demonstrated for static loads in Figure 19. Pure Mode II results have also been correlated in terms of a simplified strength of materials model (9, 10).

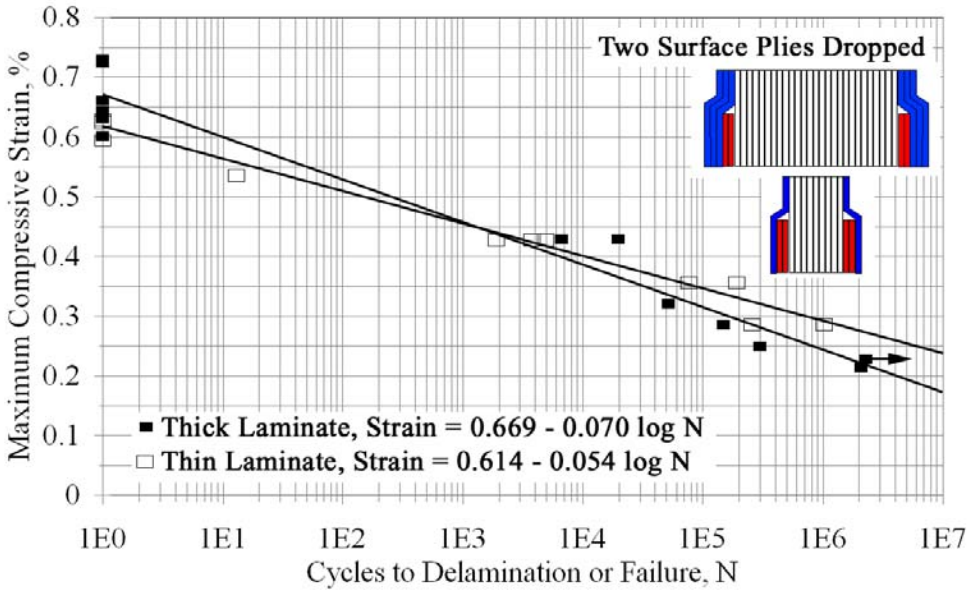

Figure 22. Comparison of strain-cycles data for a thick $[(\pm 45)_3/0_2*/0_{27}/0_2*/(\pm 45)_3]$ laminate and a thin $[\pm 45/0_2*/0_9/0_2*/\pm 45]$ laminate, double surface ply drops (9,10).

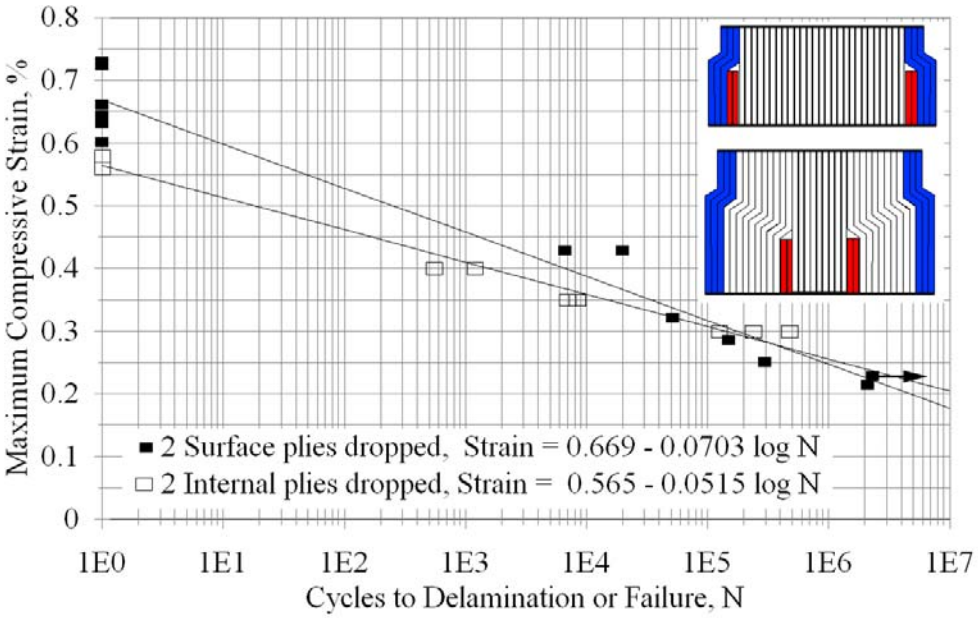

Figure 23. Comparison of strain-cycles data for surface $[(\pm 45)_3/0_2*/0_{27}/0_2*/(\pm 45)_3]$ and internal $[(\pm 45)_3/0_9/0_2*/0_9/0_2*/0_9/(\pm 45)_3]$ double ply drops, R = 10 (9,10).

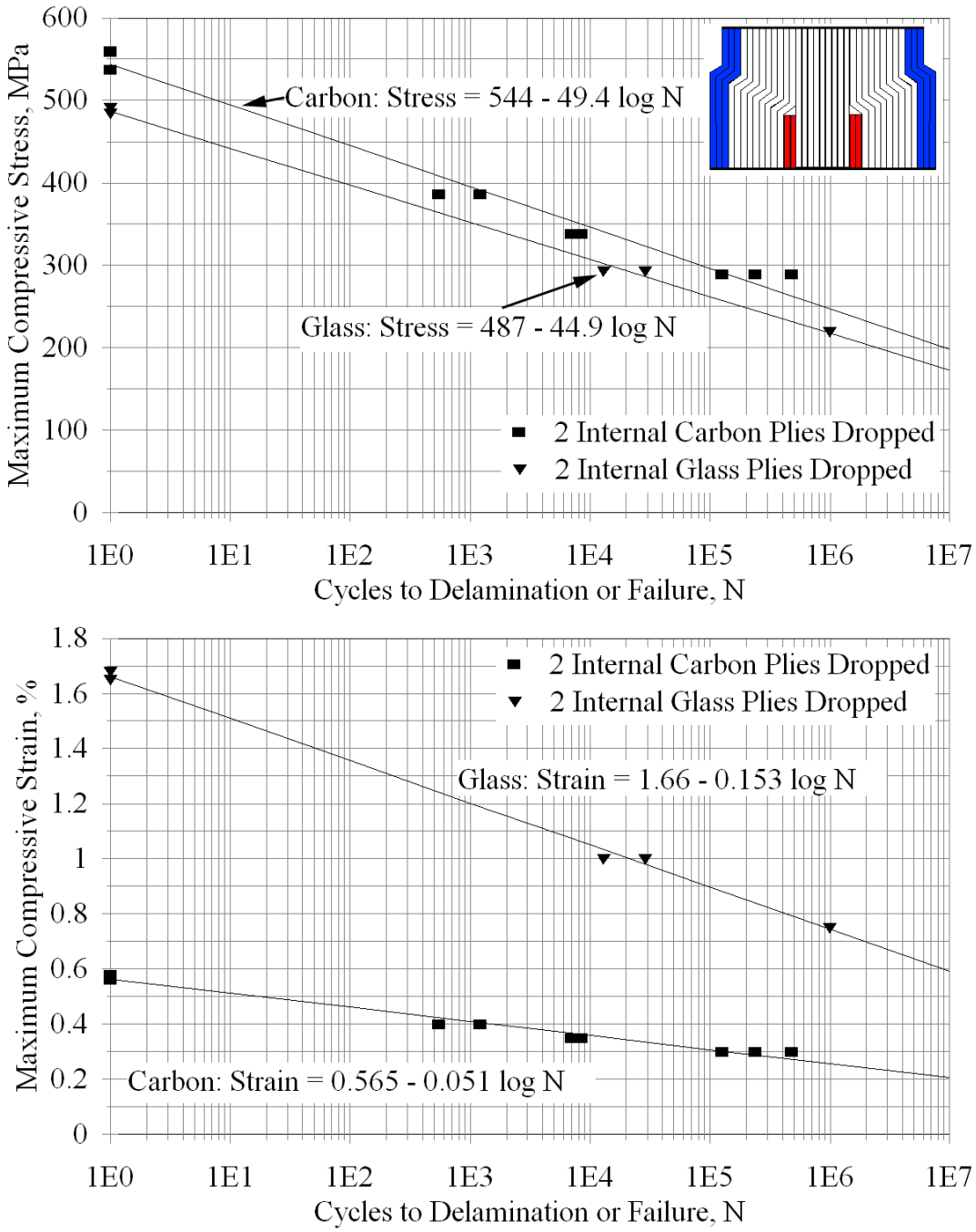

Figure 24. Stress (top) and strain-cycles comparison for laminates with carbon vs. glass 0° plies, double interior ply drops $[(\pm 45)_3/0_9/0_2*/0_9/0_2*/0_9/(\pm 45)_3]$ (±45 plies are glass).

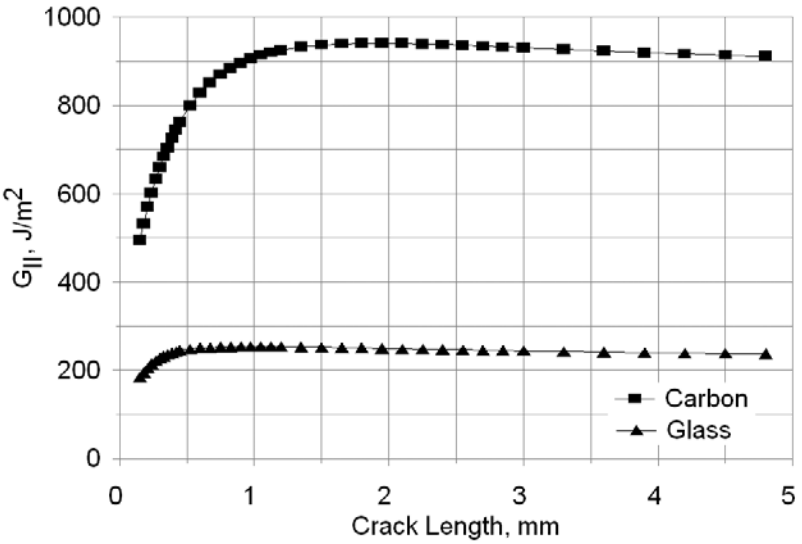

Figure 25. Comparison of glass and carbon FEA results for internal ply drop under tensile load, total G_{II} component for both cracks ($G_I \approx 0$), thin side strain = 0.5% (9).

4. CONCLUSIONS

Major issues have been identified which can produce severe fatigue damage or failure in good quality coupons at low maximum absolute strains, in the range of 0.2 to 0.4%:

1. Glass fiber laminates based on less fatigue resistant fabric architectures at higher fiber contents, loaded in tensile fatigue with R-values in the -0.5 to 0.1 range.
2. Delamination at ply drops and ply joints, for plies greater than 1.0 mm thickness for glass fibers, or 0.6 mm for carbon fibers (most R-values).
3. Matrix cracking in off-axis plies, for R-values with a significant tensile component (glass and carbon fiber laminates, various resins).

Additional issues are carbon fiber laminate compressive strength, which is sensitive to fabric or other fiber waviness, and delamination and adhesive failure in complex details under both static and fatigue loading. Hot/wet conditions can exacerbate these issues with the exception of the first.

More detailed conclusions can be found in references 7-9 and 11. Most notable are that the relatively new WindStrand^{TM} based laminates, in addition to moderately higher modulus, show very good fatigue resistance under both tension and compression loading, compared to E-glass. Carbon, either prepreg or the infused triax hybrid fabric H, is very fatigue resistant under all loading conditions; other infused fabrics have shown reduced compression resistance (2).

Delamination resistance under pure and mixed modes is strongly matrix dependent, with epoxies generally providing the most resistance (2). Ply drop delamination at high fatigue cycles occurs at low strains regardless of R-value, position through the thickness or overall laminate thickness. The important geometric parameter is the thickness of material dropped at a single position; improvements have been demonstrated (9-11) for treatments of the ply drop edge, including chamfering and pinking.

5. ACKNOWLEDGEMENTS

This work was funded by Sandia National Laboratories under several subcontracts, including Z3609. Program monitors at Sandia have included Drs. Herbert J. Sutherland, Daniel Laird and Thomas Ashwill.

6. REFERENCES

1. B. Harris, ed., Fatigue in Composites, CRC Press LLC, Boca Raton, FL, 2003, pp. 3, 36.
2. J. F. Mandell, D. D. Samborsky, and D. S. Cairns, "Fatigue of Composite Materials and Substructures for Wind Turbine Blades," Contractor Report SAND2002-0771, Sandia National Laboratories, Albuquerque, NM, 2002.
3. R. P. L. Nijssen, "Fatigue Life Prediction and Strength Degradation of Wind Turbine Rotor Blade Composites," Contractor Report SAND2006-7810P, Sandia National Laboratories, Albuquerque, NM, 2006.
4. J. F. Mandell and D. D. Samborsky, "DOE/MSU Composite Material Fatigue Database: Test Methods, Materials, and Analysis," Contractor Report SAND97-3002, Sandia National Laboratories, Albuquerque, NM, 1997.
5. J. F. Mandell and D. D. Samborsky, DOE/MSU Fatigue of Composite Materials Database. 2007 Update. (http://www.sandia.gov/wind/other/973002upd0306.pdf)
6. R. P. L. Nijssen, "OptiDAT - Fatigue of Wind Turbine Blade Materials Database," 2006, (www.kc-wmc.nl/ optimat_blades).
7. Samborsky, D. D., Wilson, T. J. and Mandell, J. F., Proc. 2007 ASME Wind Energy Symposium, Paper AIAA-07-67056, AIAA/ASME, Reno, NV, 2007.
8. D. D. Samborsky, P. Agastra and J. F. Mandell, Proc. 2008 ASME Wind Energy Symposium, Paper AIAA-2008-1346, ASME/AIAA, Reno, NV, 2008.
9. D. D. Samborsky, D. P. Avery, P. Agastra, and J. F. Mandell, Proc 2006 ASME Wind Energy Symposium, Paper AIAA-2006-1195, AIAA/ASME, Reno, NV, 2006.
10. Wilson, T.J., "Modeling of In-Plane and Interlaminar Fatigue Behavior of Glass and Carbon Fiber Composite Materials," MS Thesis, Department of Mechanical Engineering, Montana State University, 2006.
11. Global Energy Concepts, “Blade System Design Study Part II: Final Project Report,” Sandia Contractor Report, in press.
12. H. J. Sutherland and J. F. Mandell, Wind Energy, **8,** 93 (2005).
13. K. L. Reifsnider, Fatigue of Composite Materials, Elsevier, Amsterdam, 1991, pp.11-77.
14. M. Kashtalyan, in ref. 1, pp. 470-503.
15. J. F. Mandell, D. D. Samborsky, and L. Wang, SAMPE International Symposium, 48, 2653 (2003).
16. J. R. Reeder, Composite Materials: Testing and Design, STP 1206, E. T. Camponeschi, Jr., ed., American Society for Testing and Materials, Phil., 1993, pp. 303-322.
17. J. F. Mandell, D. S. Cairns, D. D. Samborsky, R. B. Morehead and D. H. Haugen, JSEE, **125**, (4), 522-530 (2003).
18. G. B. Murri, J. R. Schaff, and A. L. Dobyns," Fatigue Life Analysis of Hybrid Composite Tapered Flexbeams," NASA LaRC Technical Library Digital Repository http://hdl.handle.net/2002/15079